

DETC2015-47840

MODELING AND SIMULATION OF ASTEROID CAPTURE USING A DEFORMABLE MEMBRANE CAPTURE DEVICE

Håvard Fjær Grip, Miguel San Martin, Abhinandan Jain,
Bob Balaram, Jonathan Cameron, and Steven Myint
NASA Jet Propulsion Laboratory, California Institute of Technology
4800 Oak Grove Dr., Pasadena, California 91109

ABSTRACT

The National Aeronautics and Space Administration have recently been investigating a mission concept known as the Asteroid Redirect Mission, aimed at collecting a large amount of asteroid material and transporting it into lunar orbit for inspection by human astronauts. Of the two mission options that have been considered, one involves the capture of an entire near-Earth asteroid in the 10-m class by a robotic spacecraft. The spacecraft would first make contact with the asteroid through a deformable membrane, before securing it inside a large flexible bagging mechanism. In this paper we describe the development and implementation of a model designed for simulation of the capture process, which includes a low-complexity representation of the interaction dynamics.

INTRODUCTION

The National Aeronautics and Space Administration (NASA) has recently been investigating a mission concept known as the Asteroid Redirect Mission (ARM), aimed at collecting a large amount of asteroid material and transporting it into lunar orbit for inspection by human astronauts. Two options for gathering asteroid material have been under evaluation: in *Option A*, an entire near-Earth asteroid in the 10-m class would be captured, whereas in *Option B*, a boulder would be collected from the surface of a larger parent asteroid.¹

We focus here on the task of capturing an entire asteroid

under Option A. This task is challenging due to a number of factors, most of all the significant uncertainty that exists with respect to the mass, shape, composition, and rotational state of the eventual target asteroid. This uncertainty drives the search for a robust capture solution in terms of mechanical design and close-proximity guidance, navigation, and control (GN&C).

A particular difficulty is the complex rotational dynamics of the asteroid. Due to the large relaxation time constant of small spinning bodies [1], the asteroid is expected to tumble rather than spin about a fixed axis, inevitably resulting in non-trivial dynamical interactions as the spacecraft makes contact with the asteroid. The capture system must be designed to handle these interactions without giving rise to excessive loads on the spacecraft; of particular concern in this context are the solar array drive assemblies (SADAs), which tolerate only limited bending moments.

Capture System

An early study by the Keck Institute for Space Studies at Caltech [2] concluded that the capture of an asteroid could best be achieved by using a flexible bagging mechanism capable of fully enveloping the asteroid and securing it to the spacecraft. Such a system would be suitable both for a solid rock and a rubble pile, ensuring robustness against uncertainty in asteroid composition.

Building on this idea, a design team at NASA's Jet Propulsion Laboratory has developed a more complete concept aimed at allowing the spacecraft to establish and maintain contact with the asteroid during the bag closure, while keeping the transient dynamics and the resulting loads on the spacecraft at an acceptable

¹Since initial submission of this paper, *Option B* has been officially selected by NASA.

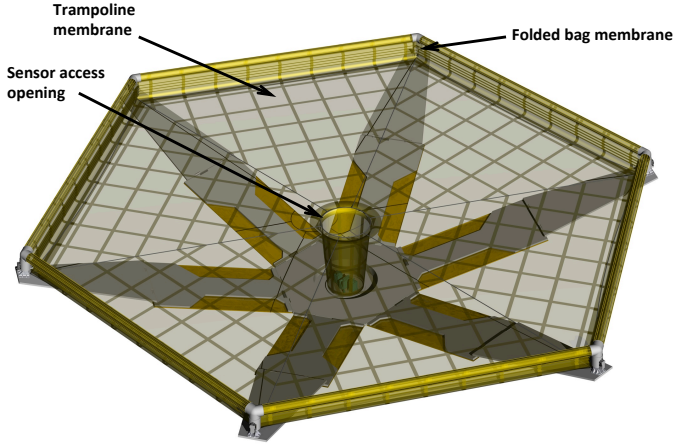


FIGURE 1. Illustration of the capture mechanism concept. The mechanism is stowed for cruise and deployed prior to capture by unfolding six “petals” supporting the hexagonal trampoline and the capture bag. The mechanism is shown here in a half-deployed state, with the capture bag still folded.

level. In this concept, the spacecraft first makes contact with the asteroid through a well-damped “trampoline,” situated within the capture bag and realized as a deformable membrane suspended from a finite number of actuated winches, as illustrated in Figure 1. Once initial contact has been made, the spacecraft applies thrust against the asteroid in order to maintain contact while the transient dynamics settle out and the capture bag closes. During this process, the trampoline acts as a shock-absorbing cushion between the spacecraft and the asteroid.

Topic of This Paper

In this paper we focus on modeling and simulation of the dynamics of the asteroid capture event, particularly during the first few minutes after contact is made through the trampoline. The goal of this effort is to provide a tool for GN&C-centric investigations of the capture problem, including the design of the approach strategy, gains, and thrust levels, as well as large-scale explorations of parameters and initial conditions through Monte-Carlo simulations.

Methods for simulating elastic membranes include finite-element models and spring meshes (see, e.g., [3] and references therein). These types of approaches result in high-order models whose computational requirements can be prohibitive for the purposes outlined above. We therefore choose a simplified approach that *ignores* the dynamics of the trampoline. At any given time, the shape of the trampoline is taken as a function only of the instantaneous relative pose of the asteroid and the trampoline suspension points, the implicit assumption being that any internal dynamics in the trampoline evolve and settle on a time scale

much faster than the remaining dynamics of the system.

The shape of the trampoline, as a function of the relative pose of the asteroid and the trampoline suspension points, is estimated based on a convex hull. To compute the forces and torques arising from the interaction, we associate with a given deflection of the trampoline a particular potential energy, and with a given rate of deflection a loss of energy due to viscoelastic damping, similar in principle to the modeling of a linear spring-damper. Based on the resulting energy balance and the conservation of momentum, we calculate restoring and damping forces, and augment these with friction forces based on a Coulomb friction model distributed across points on the contact surface.

Clearly, the modeling procedure described above involves a level of abstraction away from the actual mechanical implementation of the trampoline. In particular, we make certain assumptions regarding how the trampoline responds to deflections in terms of the storage of potential energy and loss of energy due to damping. We note, however, that the mechanization of the trampoline, using actively controlled winches, provides considerable flexibility in shaping the response of the trampoline to meet requirements that may be derived through simulation. Conversely, it is possible to modify the properties of the simulated trampoline by applying different profiles for potential energy and viscoelastic damping.

For additional context on the asteroid capture problem, we refer the reader to an earlier paper [4], which discusses prior generations of the capture system concept as well as simulation studies aimed at determining feasibility of the capture problem.

NOMENCLATURE

In our derivations we shall use multiple frames of reference interchangeably. We use superscripts to indicate the frame of reference for a particular two- or three-dimensional vector; for example, x^a refers to the vector x decomposed in frame a . The rotation matrix from frame a to frame b is denoted by R_a^b , so that $R_a^b x^a = x^b$. We denote by ω_{ab}^c the angular velocity of frame b with respect to frame a , decomposed in frame c .

For a vector $x \in \mathbb{R}^3$, we denote by $S(x)$ the skew-symmetric matrix such that for any $y \in \mathbb{R}^3$, $S(x)y = x \times y$. For a scalar $x \in \mathbb{R}$, we define $S(x) = \begin{bmatrix} 0 & -x \\ x & 0 \end{bmatrix}$.

TRAMPOLINE MODEL

In this section we describe the derivation of the trampoline model that will be used as part of the asteroid capture simulation. For clarity of presentation, we describe the derivation of a 2D model before extending the same modeling principles to the 3D case.

2D Model

We consider here a two-dimensional trampoline suspended at two fixed points, together with a rigid body that can come in contact with the trampoline. Our goal is to model the forces and torques acting on the body as a result of this contact, thus allowing us to simulate the evolution of the state of the body over time. We assume that the body shape is described by a two-dimensional polygon, represented by an ordered set of vertices. The body is free to move in two-dimensional space, as described by the following dynamical system:

$$\begin{aligned}\dot{p}^i &= R_b^i v^b, \\ m\dot{v}^b &= -mS(\omega_{ib})v^b + f^b, \\ \dot{R}_b^i &= R_b^i S(\omega_{ib}), \\ J\dot{\omega}_{ib} &= \tau,\end{aligned}$$

where $p^i \in \mathbb{R}^2$ is the position of the body center of mass (CM), decomposed in the *inertial reference frame* i ; $v^b \in \mathbb{R}^2$ is the velocity of the CM, decomposed in the *body-fixed frame* b ; $R_b^i \in \text{SO}(2)$ is the rotation matrix from the body-fixed frame to the inertial frame; $\omega_{ib} \in \mathbb{R}$ is the angular rate of the body-fixed frame relative to the inertial reference frame; $f^b \in \mathbb{R}^2$ and $\tau \in \mathbb{R}$ are the forces and torques acting on the body; and $m \in \mathbb{R}$ and $J \in \mathbb{R}$ are the mass and inertia of the body. The modeling task at hand consists of determining f^b and τ as a function of the state of the system. For the purpose of the remaining discussion, we assume that f^b and τ are the result only of interactions with the trampoline; other forces (such as gravity) can be added as desired.

Trampoline Shape As discussed in the introduction, we do not model the internal dynamics of the trampoline; instead, we assume that the shape of the trampoline is a function of the pose of the body relative to the trampoline suspension points. In particular, to estimate the shape, we take the *convex hull* of the suspension points of the trampoline and the vertices of the body that are located *below* the straight line connecting the trampoline suspension points.² From the boundary of the convex hull, described as a finite set of line segments, we remove the segment connecting the two suspension points to arrive at our estimate of the trampoline shape. Figure 2 illustrates the result of this process.

Let $\ell = \sum_{j=1}^n \ell_j$ denote the length of the trampoline, where ℓ_j denotes the length of a single segment, in order from left to right (see Figure 2). Note that the number of segments n varies with time. The rate of change in ℓ can be computed as $\dot{\ell} = \sum_{j=1}^n \dot{\ell}_j =$

²If no vertices are located below the line connecting the suspension points, then the body is not in contact with the trampoline and no forces act on the body; the remainder of this derivation assumes contact between the body and the trampoline.

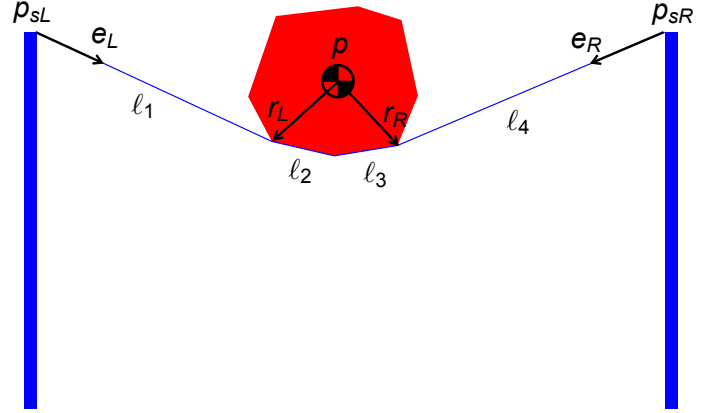


FIGURE 2. The figure shows the trampoline shape obtained by taking the convex hull of the trampoline suspension points and the vertices of the rigid body located below the suspension points.

$\dot{\ell}_1 + \dot{\ell}_n$, where we have used the fact that $\ell_2, \dots, \ell_{n-1}$ represent segments connecting vertices of the rigid body, whose lengths do not change with time.

We are interested in writing $\dot{\ell}$ as a function of the state variables of the system. To this end, let p_{sL}^i and p_{sR}^i denote the positions of the left and right suspension points, respectively. Furthermore, let r_L^b denote the constant vector from the CM of the rigid body to the leftmost vertex in contact with the trampoline. Similarly, let r_R^b denote the vector from the CM to the rightmost vertex in contact with the trampoline. We can now write $\ell_1 = \|p^i + R_b^i r_L^b - p_{sL}^i\|$. Hence,

$$\begin{aligned}\dot{\ell}_1 &= \frac{(p^i + R_b^i r_L^b - p_{sL}^i)^\top (\dot{p}^i + \dot{R}_b^i r_L^b)}{\ell_1} = e_L^i{}^\top (R_b^i v^b + R_b^i S(\omega_{ib}) r_L^b) \\ &= e_L^i{}^\top (v^i + S(\omega_{ib}) r_L^i),\end{aligned}$$

where e_L^i is the unit vector pointing from p_{sL}^i to $p^i + R_b^i r_L^b$, and where we have used the identity $R_b^i S(x) = S(x) R_b^i$ for an arbitrary scalar x . Similarly, we can write $\dot{\ell}_n = e_R^i{}^\top (v^i + S(\omega_{ib}) r_R^i)$, where e_R^i is the unit vector pointing from p_{sR}^i to $p^i + R_b^i r_R^b$. We can now write $\dot{\ell} = e_L^i{}^\top (v^i + S(\omega_{ib}) r_L^i) + e_R^i{}^\top (v^i + S(\omega_{ib}) r_R^i)$.

Restoring and Damping Forces We decompose the forces and torques in the body reference frame as $f^b = f_N^b + f_f^b$ and $\tau = \tau_N + \tau_f$. The force f_N^b and the torque τ_N represent *normal forces* and corresponding torques, which arise due to the trampoline's resistance to deflection and viscoelastic damping due to changes in deflection. The force f_f and the torque τ_f represent *friction forces* and corresponding torques.

We start by modeling f_N^b and τ_N , temporarily letting $f_f^b = 0$ and $\tau_f = 0$. We assume that the trampoline, when deformed,

responds in a manner similar to a linear spring-damper; in particular,

1. the trampoline has a potential energy equal to $\frac{1}{2}k(\ell - \ell_0)^2$, where $k > 0$ is a constant, and $\ell_0 = \|p_{sR}^i - p_{sL}^i\|$ is the nominal length of the trampoline; and
2. the system experiences a loss of energy from viscoelastic damping equal to $-c\dot{\ell}^2$, where $c > 0$ is a damping constant.

Consider now the total kinetic and potential energy of the system:

$$E = \frac{1}{2}k(\ell - \ell_0)^2 + \frac{1}{2}mv^{b\top}v^b + \frac{1}{2}J\omega_{ib}^2.$$

The rate of change in energy is

$$\begin{aligned}\dot{E} &= k(\ell - \ell_0)\dot{\ell} + v^{b\top}f_N^b + \omega_{ib}\tau_N \\ &= k(\ell - \ell_0)\left(v^{i\top}(e_L^i + e_R^i)\right. \\ &\quad \left. - r_L^{i\top}S(\omega_{ib})e_L^i - r_R^{i\top}S(\omega_{ib})e_R^i\right) + v^{i\top}f_N^i + \omega_{ib}\tau_N.\end{aligned}$$

Since the forces on the rigid body are due to reaction at the trampoline suspension points and act through the trampoline fabric, they can be decomposed as two forces of magnitude F_L and F_R along the unit vectors e_L^i and e_R^i : $f_N^i = f_L^i + f_R^i = F_L e_L^i + F_R e_R^i$. It is easy to confirm that the torque associated with these forces is given by

$$\begin{aligned}\tau_N &= \tau_L + \tau_R = -r_L^{i\top}S(1)f_L^i - r_R^{i\top}S(1)f_R^i \\ &= -F_L r_L^{i\top}S(1)e_L^i - F_R r_R^{i\top}S(1)e_R^i.\end{aligned}$$

Expanding the desired expression $\dot{E} = -c\dot{\ell}^2$ for the rate of energy loss, we now obtain

$$\begin{aligned}k(\ell - \ell_0)\left(v^{i\top}(e_L^i + e_R^i) - r_L^{i\top}S(\omega_{ib})e_L^i - r_R^{i\top}S(\omega_{ib})e_R^i\right) \\ + v^{i\top}(F_L e_L^i + F_R e_R^i) - F_L r_L^{i\top}S(\omega_{ib})e_L^i - F_R r_R^{i\top}S(\omega_{ib})e_R^i \\ = -c\dot{\ell}\left(v^{i\top}(e_L^i + e_R^i) - r_L^{i\top}S(\omega_{ib})e_L^i - r_R^{i\top}S(\omega_{ib})e_R^i\right).\end{aligned}$$

It is easy to verify that this equation is solved by $F_L = F_R = -k(\ell - \ell_0) - c\dot{\ell}$. Hence, the normal force and corresponding torque on the rigid body are given by

$$\begin{aligned}f_N^b &= -(k(\ell - \ell_0) + c\dot{\ell})(e_L^b + e_R^b), \\ \tau_N &= (k(\ell - \ell_0) + c\dot{\ell})(r_L^{b\top}S(1)e_L^b + r_R^{b\top}S(1)e_R^b).\end{aligned}$$

Friction Force Modeling In addition to the restoring and viscoelastic damping forces, the body will be subject to friction forces as it slides against the trampoline surface. Friction phenomena are highly complex and difficult to model in general, and more so when a deformable trampoline surface is involved. We base ourselves on the simple but commonly applied Coulomb friction model, in which the friction between two sliding surfaces is modeled as $f_f = -\mu F_N e_s$, where μ is the coefficient of friction, F_N is the normal force between the surfaces, and e_s is the unit vector pointing in the direction of sliding.

In many cases the system being modeled involves bodies that are in contact at several places or over a surface area with a non-uniform friction coefficient or sliding direction. In these cases, it is common to distribute the total normal force over a distributed set of reference points and to apply the Coulomb friction model separately at each point. We choose a similar strategy here.

For each vertex of the rigid body that is in contact with the trampoline (i.e., that is included in the convex hull), we define two unit vectors normal to the two line segments joined at that vertex. The result is a set of unit vectors n_1^b, \dots, n_m^b , which we use to distribute the total normal force across the corresponding vertices. To this end, we need to find F_{N1}, \dots, F_{Nm} , such that the following holds:

$$f_N^b = \sum_{j=1}^m F_{Nj} n_j^b, \quad \tau = -\sum_{j=1}^m F_{Nj} r_j^{b\top} S(1) n_j^b,$$

where r_j^b represents the vector from the CM of the body to the vertex corresponding to vector n_j^b .

The above expression gives rise to the generally underdetermined set of equations

$$\begin{bmatrix} n_1^b & \dots & n_m^b \\ -r_1^{b\top}S(1)n_1^b & \dots & -r_m^{b\top}S(1)n_m^b \end{bmatrix} \begin{bmatrix} F_{N1} \\ \vdots \\ F_{Nm} \end{bmatrix} = \begin{bmatrix} f_N^b \\ \tau_N \end{bmatrix}.$$

In order to solve the above for the normal forces that are non-negative, a complementarity problem can be posed [5–7] and subsequently solved to obtain the solution. We instead choose a less robust but faster approach based on the Moore-Penrose pseudoinverse. This approach has the drawback of potentially generating illegal solutions that contain negative normal forces; in our implementation, a check was therefore added to verify that the solutions were legal.

Based on the computed normal forces, the Coulomb friction model is now applied twice at each vertex in contact with the trampoline, once for each of the normal vectors originating there. The sliding velocity is in each case computed by projecting



FIGURE 3. The figure shows the trampoline shape obtained by taking the convex hull of the trampoline suspension points and the vertices of the rigid body located below the suspension points.

the velocity of the vertex onto the line segment from which the normal vector was derived. The torques arising from the friction forces are computed in the obvious way.

3D Model

We now extend the modeling technique to the 3D case. We assume that the body shape is described as a polygon mesh, in the form of a finite set of vertices joined by triangular surfaces. The dynamics of the body is now described by the following Newton-Euler equations of motion:

$$\begin{aligned}\dot{p}^i &= R_b^i v^b, \\ m\dot{v}^b &= -mS(\omega_{ib}^b)v^b + f^b, \\ \dot{R}_b^i &= R_b^i S(\omega_{ib}^b), \\ J\dot{\omega}_{ib}^b &= -S(\omega_{ib}^b)J\omega_{ib}^b + \tau^b,\end{aligned}$$

where $p^i \in \mathbb{R}^3$ is the position of the body's CM in the inertial reference frame; $v^b \in \mathbb{R}^3$ is the velocity at the CM with respect to a body-fixed reference frame; $R_b^i \in \text{SO}(3)$ is the rotation matrix from the body-fixed frame to the inertial frame; $\omega_{ib}^b \in \mathbb{R}^3$ is the angular velocity of the body-fixed frame with respect to the inertial frame; $f^b \in \mathbb{R}^3$ and $\tau^b \in \mathbb{R}^3$ are the forces and the torques acting on the body; $m \in \mathbb{R}$ is the mass; and $J \in \mathbb{R}^{3 \times 3}$ is the inertia.

Trampoline Shape Similar to the 2D case, we estimate the shape of the trampoline by the convex hull of the trampoline suspension points and the vertices of the body located below the trampoline surface. From the boundary of the convex hull, now described by a set of triangles, we remove those triangles that are formed only from trampoline suspension points, to arrive at our estimate of the trampoline shape. Figure 3 illustrates the result of this process.

Let $A = \sum_{j=1}^n A_j$ denote the area of the trampoline, where A_j denotes the area of a single triangle forming part of the trampoline. The area of a single triangle is given by $A_j = \frac{1}{2} \|\rho_{j1}^i \times \rho_{j2}^i\|$,

where ρ_{j1}^i and ρ_{j2}^i are vectors corresponding to two of the triangle's three sides.

Observing the fact that triangles joining only vertices of the rigid body are of constant area, the rate of change in A can be computed as $\dot{A} = \sum_{j \in \mathcal{S}} \dot{A}_j$, where $\mathcal{S} \subset 1, \dots, n$ enumerates those triangles for which at least one endpoint corresponds to a trampoline suspension point.

To calculate A_j , $j \in \mathcal{S}$, as a function of the state variables of the system, let the vectors ρ_{j1}^i and ρ_{j2}^i be chosen such that both originate at trampoline suspension points, located at p_{sj1}^i and p_{sj2}^i , respectively (see Figure 4). Furthermore, let r_{j1}^b and r_{j2}^b denote the respective vectors from the CM to the asteroid vertices that form the endpoints of ρ_{j1}^i and ρ_{j2}^i . Then $\rho_{j1}^i = p^i + R_b^i r_{j1}^b - p_{sj1}^i$ and $\rho_{j2}^i = p^i + R_b^i r_{j2}^b - p_{sj2}^i$; moreover, $\dot{\rho}_{j1}^i = R_b^i v^b + R_b^i S(\omega_{ib}^b) r_{j1}^b = v^i + S(\omega_{ib}^i) r_{j1}^i$ and $\dot{\rho}_{j2}^i = R_b^i v^b + R_b^i S(\omega_{ib}^b) r_{j2}^b = v^i + S(\omega_{ib}^i) r_{j2}^i$, where we have used the identity $R_b^i S(x^b) = S(x^i) R_b^i$ for $x \in \mathbb{R}^3$. Based on this, it is straightforward to calculate

$$\begin{aligned}A_j &= \frac{(\rho_{j1}^i \times \rho_{j2}^i)^\top}{4A_j} (S(\rho_{j1}^i - \rho_{j2}^i) v^i \\ &\quad + (S(\rho_{j2}^i) S(r_{j1}^i) - S(\rho_{j1}^i) S(r_{j2}^i)) \omega_{ib}^i).\end{aligned}$$

Restoring and Damping Forces As in the 2D case we decompose the forces and torques as $f^b = f_N^b + f_f^b$ and $\tau^b = \tau_N^b + \tau_f^b$, and start by modeling f_N^b and τ_N^b . We associate a potential energy with a deflection of the trampoline from the nominal, and an energy loss with a change in deflection; however, the deflection is now described in terms of the trampoline *area*. In particular, we assume that

1. the trampoline has a potential energy equal to $\frac{1}{2}k(A - A_0)^2$, where $k > 0$ is a constant, and A_0 is the nominal area of the undeflected trampoline; and
2. the system experiences a loss of energy from viscoelastic damping equal to $-c\dot{A}^2$, where $c > 0$ is a damping constant.

Consider now the total kinetic and potential energy of the system:

$$E = \frac{1}{2}k(A - A_0)^2 + \frac{1}{2}mv^b{}^\top v^b + \frac{1}{2}\omega_{ib}^b{}^\top J\omega_{ib}^b.$$

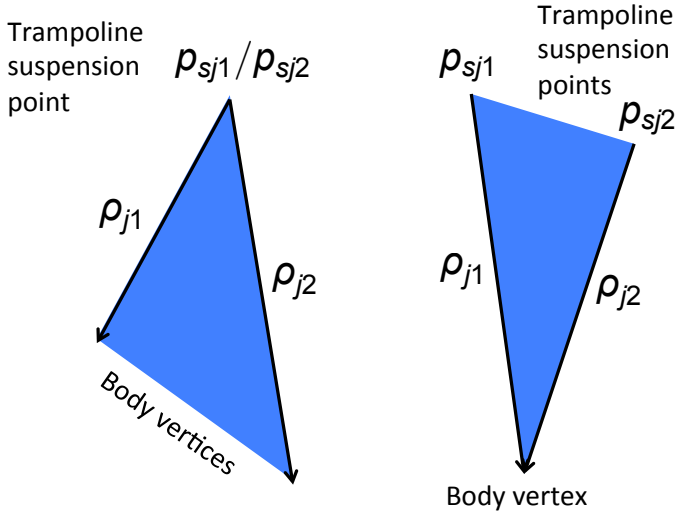


FIGURE 4. Triangles connecting trampoline suspension points to body vertices either contain a single suspension point and two body vertices (left) or two suspension points and a single body vertex (right).

The rate of change in energy is

$$\begin{aligned}
\dot{E} &= k(A - A_0)\dot{A} + v^{bT} f_N^b + \omega_{ib}^{bT} \tau_N^b \\
&= k(A - A_0) \left(-v^{iT} \sum_{j \in \mathcal{J}} \frac{1}{4A_j} S(\rho_{j1}^i - \rho_{j2}^i) (\rho_{j1}^i \times \rho_{j2}^i) \right. \\
&\quad \left. + \omega_{ib}^{iT} \sum_{j \in \mathcal{J}} \frac{1}{4A_j} (S(r_{j1}^i) S(\rho_{j2}^i) - S(r_{j2}^i) S(\rho_{j1}^i)) (\rho_{j1}^i \times \rho_{j2}^i) \right) \\
&\quad + v^{iT} f_N^i + \omega_{ib}^{iT} \tau_N^i.
\end{aligned}$$

Since the forces on the rigid body are due to reaction at the trampoline suspension points and are transmitted through the trampoline fabric, they can be decomposed as n forces, $f_N^i = \sum_{j \in \mathcal{J}} f_{Nj}^i$, one for each triangle connecting the suspension points to the rigid body. Each force f_{Nj}^i is in turn decomposed as a sum of forces acting along the vectors ρ_{j1}^i and ρ_{j2}^i : $f_{Nj}^i = f_{Nj1}^i + f_{Nj2}^i = F_{j1} e_{j1}^i + F_{j2} e_{j2}^i$, where $e_{j1}^i = \rho_{j1}^i / \|\rho_{j1}^i\|$ and $e_{j2}^i = \rho_{j2}^i / \|\rho_{j2}^i\|$. The torque arising from these forces is similarly decomposed as $\tau_N^i = \sum_{j \in \mathcal{J}} \tau_{Nj}^i$, where $\tau_{Nj}^i = \tau_{Nj1}^i + \tau_{Nj2}^i = F_{j1} S(r_{j1}^i) e_{j1}^i + F_{j2} S(r_{j2}^i) e_{j2}^i$.

Expanding the desired expression $\dot{E} = -c\dot{A}^2$ for the rate of energy loss, we now obtain

$$\begin{aligned}
k(A - A_0) &\left(-v^{iT} \sum_{j \in \mathcal{J}} \frac{1}{4A_j} S(\rho_{j1}^i - \rho_{j2}^i) (\rho_{j1}^i \times \rho_{j2}^i) \right. \\
&\quad \left. + \omega_{ib}^{iT} \sum_{j \in \mathcal{J}} \frac{1}{4A_j} (S(r_{j1}^i) S(\rho_{j2}^i) - S(r_{j2}^i) S(\rho_{j1}^i)) (\rho_{j1}^i \times \rho_{j2}^i) \right) \\
&+ v^{iT} \sum_{j \in \mathcal{J}} (F_{j1} e_{j1}^i + F_{j2} e_{j2}^i) + \omega_{ib}^{iT} \sum_{j \in \mathcal{J}} (F_{j1} S(r_{j1}^i) e_{j1}^i + F_{j2} S(r_{j2}^i) e_{j2}^i) \\
&= -c\dot{A} \left(-v^{iT} \sum_{j \in \mathcal{J}} \frac{1}{4A_j} S(\rho_{j1}^i - \rho_{j2}^i) (\rho_{j1}^i \times \rho_{j2}^i) \right. \\
&\quad \left. + \omega_{ib}^{iT} \sum_{j \in \mathcal{J}} \frac{1}{4A_j} (S(r_{j1}^i) S(\rho_{j2}^i) - S(r_{j2}^i) S(\rho_{j1}^i)) (\rho_{j1}^i \times \rho_{j2}^i) \right).
\end{aligned}$$

Clearly this equation can be solved if we can solve the following individual equation for each $j \in 1, \dots, n$:

$$\begin{aligned}
v^{iT} (F_{j1} e_{j1}^i + F_{j2} e_{j2}^i) + \omega_{ib}^{iT} (F_{j1} S(r_{j1}^i) e_{j1}^i + F_{j2} S(r_{j2}^i) e_{j2}^i) \\
= \frac{a}{4A_j} \left(v^{iT} S(\rho_{j1}^i - \rho_{j2}^i) (\rho_{j1}^i \times \rho_{j2}^i) \right. \\
\left. - \omega_{ib}^{iT} (S(r_{j1}^i) S(\rho_{j2}^i) - S(r_{j2}^i) S(\rho_{j1}^i)) (\rho_{j1}^i \times \rho_{j2}^i) \right),
\end{aligned}$$

where $a := k(A - A_0) + c\dot{A}$. This equation is in turn solved if we can find a common solution to the following individual equations:

$$F_{j1} e_{j1}^i + F_{j2} e_{j2}^i = \frac{a}{4A_j} S(\rho_{j1}^i - \rho_{j2}^i) (\rho_{j1}^i \times \rho_{j2}^i) \quad (1)$$

and

$$\begin{aligned}
F_{j1} S(r_{j1}^i) e_{j1}^i + F_{j2} S(r_{j2}^i) e_{j2}^i \\
= -\frac{a}{4A_j} (S(r_{j1}^i) S(\rho_{j2}^i) - S(r_{j2}^i) S(\rho_{j1}^i)) (\rho_{j1}^i \times \rho_{j2}^i). \quad (2)
\end{aligned}$$

We will start by solving (1); we will then show that the solution is also a solution of (2).

Equation (1) can be rewritten as

$$[e_{j1}^i \ e_{j2}^i] \begin{bmatrix} F_{j1} \\ F_{j2} \end{bmatrix} = -\frac{a}{2} S(e_j^i) (\rho_{j1}^i - \rho_{j2}^i), \quad (3)$$

where $e_j^i = e_{j1}^i \times e_{j2}^i$. Pre-multiplying by the non-singular matrix $[e_{j1}^i, e_{j2}^i, e_j^i]^T$ and noting that $e_j^{iT} e_{j1}^i = 0$, $e_j^{iT} e_{j2}^i = 0$, $e_j^{iT} S(e_j^i) = 0$,

$e_{j1}^i \top e_{j1}^i = 1$, and $e_{j2}^i \top e_{j2}^i = 1$, we obtain the equivalent equation

$$\begin{bmatrix} 1 & b \\ b & 1 \\ 0 & 0 \end{bmatrix} \begin{bmatrix} F_{j1} \\ F_{j2} \end{bmatrix} = -\frac{a}{2} \begin{bmatrix} e_{j1}^i \top \\ e_{j2}^i \top \\ 0 \end{bmatrix} S(e_j^i)(\rho_{j1}^i - \rho_{j2}^i),$$

where $b := e_{j1}^i \top e_{j2}^i$. Eliminating and inverting the resulting left-most matrix yields

$$\begin{aligned} \begin{bmatrix} F_{j1} \\ F_{j2} \end{bmatrix} &= -\frac{a}{2(1-b^2)} \begin{bmatrix} 1 & -b \\ -b & 1 \end{bmatrix} \begin{bmatrix} e_{j1}^i \top \\ e_{j2}^i \top \end{bmatrix} S(e_j^i)(\rho_{j1}^i - \rho_{j2}^i) \\ &= -\frac{a}{2(1-b^2)} \begin{bmatrix} e_{j1}^i \top (I - e_{j2}^i e_{j2}^i \top) \\ e_{j2}^i \top (I - e_{j1}^i e_{j1}^i \top) \end{bmatrix} S(e_j^i)(\rho_{j1}^i - \rho_{j2}^i). \end{aligned}$$

Expanding the expression, this yields the forces

$$\begin{aligned} f_{Nj1}^i &= -\frac{k(A-A_0) + c\dot{A}}{2(1-(e_{j1}^i \top e_{j2}^i)^2)} e_{j1}^i e_{j1}^i \top (I - e_{j2}^i e_{j2}^i \top) S(e_j^i)(\rho_{j1}^i - \rho_{j2}^i), \\ f_{Nj2}^i &= -\frac{k(A-A_0) + c\dot{A}}{2(1-(e_{j1}^i \top e_{j2}^i)^2)} e_{j2}^i e_{j2}^i \top (I - e_{j1}^i e_{j1}^i \top) S(e_j^i)(\rho_{j1}^i - \rho_{j2}^i). \end{aligned}$$

Next, we show that this solution also satisfies (2). To this end, we first note that (2) can be rewritten as

$$\begin{aligned} [S(r_{j1}^i) e_{j1}^i \ S(r_{j2}^i) e_{j2}^i] \begin{bmatrix} F_{j1} \\ F_{j2} \end{bmatrix} \\ = -\frac{a}{2} (S(r_{j1}^i) S(\rho_{j2}^i) - S(r_{j2}^i) S(\rho_{j1}^i)) e_j^i. \end{aligned} \quad (4)$$

We now consider two distinct possibilities: (i) triangle j includes two trampoline suspension points; and (ii) triangle j includes two body vertices (see Figure 4). In the first case, $r_{j1}^i = r_{j2}^i$, and hence we can write (4) as

$$\begin{aligned} S(r_{j1}^i) [e_{j1}^i \ e_{j2}^i] \begin{bmatrix} F_{j1} \\ F_{j2} \end{bmatrix} &= -S(r_{j1}^i) \frac{a}{2} S(\rho_{j2}^i - \rho_{j1}^i) e_j^i \\ &= -S(r_{j1}^i) \frac{a}{2} S(e_j^i)(\rho_{j1}^i - \rho_{j2}^i). \end{aligned}$$

It is easy to see that this equation is satisfied since (3) is satisfied. In the second case, we can write $r_{j1}^i = s_j^i + \rho_{j1}^i$ and $r_{j2}^i = s_j^i + \rho_{j2}^i$, where s_j^i is the trampoline suspension point included in triangle j . Noting that $S(\rho_{j1}^i) e_{j1}^i = 0$ and $S(\rho_{j2}^i) e_{j2}^i = 0$ we can rewrite

(4) as

$$\begin{aligned} S(s_j^i) [e_{j1}^i \ e_{j2}^i] \begin{bmatrix} F_{j1} \\ F_{j2} \end{bmatrix} \\ = -\frac{a}{2} (S(s_j^i + \rho_{j1}^i) S(\rho_{j2}^i) - S(s_j^i + \rho_{j2}^i) S(\rho_{j1}^i)) e_j^i \\ = -S(s_j^i) \frac{a}{2} S(e_j^i)(\rho_{j1}^i - \rho_{j2}^i) \\ - \frac{a}{2} (S(\rho_{j1}^i) S(\rho_{j2}^i) - S(\rho_{j2}^i) S(\rho_{j1}^i)) e_j^i. \end{aligned}$$

Considering the factor $(S(\rho_{j1}^i) S(\rho_{j2}^i) - S(\rho_{j2}^i) S(\rho_{j1}^i)) e_j^i$ in the last term, we can write

$$\begin{aligned} (S(\rho_{j1}^i) S(\rho_{j2}^i) - S(\rho_{j2}^i) S(\rho_{j1}^i)) e_j^i \\ = \frac{1}{2A_j} (S(\rho_{j1}^i) S(\rho_{j2}^i) - S(\rho_{j2}^i) S(\rho_{j1}^i)) (\rho_{j1}^i \times \rho_{j2}^i) \\ = \frac{1}{2A_j} (S(\rho_{j1}^i) S(\rho_{j2}^i) S(\rho_{j1}^i) \rho_{j2}^i - S(\rho_{j2}^i) S(\rho_{j1}^i)^2 \rho_{j2}^i) \\ = \frac{1}{2A_j} (-S(\rho_{j1}^i) S(\rho_{j2}^i)^2 \rho_{j1}^i - S(\rho_{j2}^i) S(\rho_{j1}^i)^2 \rho_{j2}^i) = 0, \end{aligned}$$

where we have used the identity $S(x)S(y)^2x = -S(y)S(x)^2y$. It now follows that

$$S(s_j^i) [e_{j1}^i \ e_{j2}^i] \begin{bmatrix} F_{j1} \\ F_{j2} \end{bmatrix} = -S(s_j^i) \frac{a}{2} S(e_j^i)(\rho_{j1}^i - \rho_{j2}^i),$$

which is satisfied since (3) is satisfied.

Friction Force Modeling The modeling of friction forces is carried out in the same way as for the 2D case. For each vertex of the body that is in contact with the trampoline, we define a normal vector based on each adjacent triangular surface, and we use the collection of all the normal vectors to distribute the normal force calculated in the previous section. For each of these normal forces, Coulomb's friction model is then applied at the corresponding vertex, with the sliding direction calculated by projecting the velocity of the vertex onto the surface from which the normal vector was calculated.

Simulation Figure 5 shows a sequence of images from a Matlab simulation in which a 100-kg object with a maximum diameter of approximately 4.5 m falls in Earth gravity and bounces off the trampoline. The hexagonal trampoline has a nominal area of approximately 146 m² and is parameterized with $k = 30$ N/m³, $c = 1.5$ Ns/m³, and $\mu = 0.2$. The object has a tri-inertial mass geometry and is initialized in a tumbling rotational state.

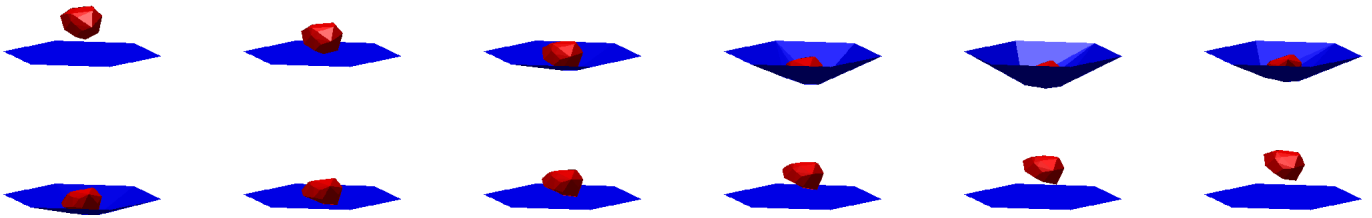


FIGURE 5. Excerpt from Matlab simulation of an object bouncing off a trampoline in Earth gravity. The object was dropped from a height of 10 m above the trampoline with an angular velocity of $\omega_{ib}^b = [0.5, 1.0, -0.2]^T$ rad/s. The images show the period from $t = 1.2$ s to $t = 2.52$ s in 0.12 s increments, in order from top left to top right, continuing from bottom left to bottom right.

ASTEROID CAPTURE

The ARM Option A mission concept, as outlined in the introduction, consists of two elements: an unmanned robotic mission to capture an asteroid and bring it into lunar orbit, and a manned mission to visit the asteroid in lunar orbit. The spacecraft that would be to accomplish the robotic mission, referred to as the Asteroid Retrieval Vehicle (ARV), consists of a hexagonal central bus approximately 3 m in diameter and 6 m in height and with a mass of approximately 15 t, with the asteroid capture device mounted at one end (see Figure 6). Two large solar panels are used to power the ARV’s solar-electric propulsion system. Each solar panel is carried on a boom mounted on a gimbal mechanism known as a solar array drive assembly (SADA). Mechanically, the SADAs represent a weak point on the spacecraft, as they can tolerate only limited bending moments during the asteroid capture event.

Potential asteroid targets, limited by the dimensions of the capture bag and the propulsive capacity of the spacecraft, may measure up to 13 m in diameter and have a mass of up to 1000 t. While the asteroid is expected to tumble, the instantaneous spin rate of any potential target will be within known limits. In [4] it was shown that a properly designed capture mechanism may be capable of handling a tumbling asteroid rotating at 2 RPM without exceeding an assumed SADA bending moment limit of 1765 Nm. However, the margins in this scenario were small for certain types of rotational patterns. The requirement on the target spin rate was since reduced to 0.5 RPM.

Approach Strategy As discussed in [4], the transient dynamics of the combined asteroid-spacecraft system after contact is to a large extent determined by the strategy chosen for approaching the asteroid. Due to the possibly complicated rotational state and *a priori* unknown asteroid shape, choosing the optimal approach strategy is nontrivial. Key considerations include minimizing the relative motion between the spacecraft and the asteroid at the time of contact; ensuring sufficient thruster leverage for subsequent despin; keeping the asteroid relatively centered in the bag during approach; and minimizing transients

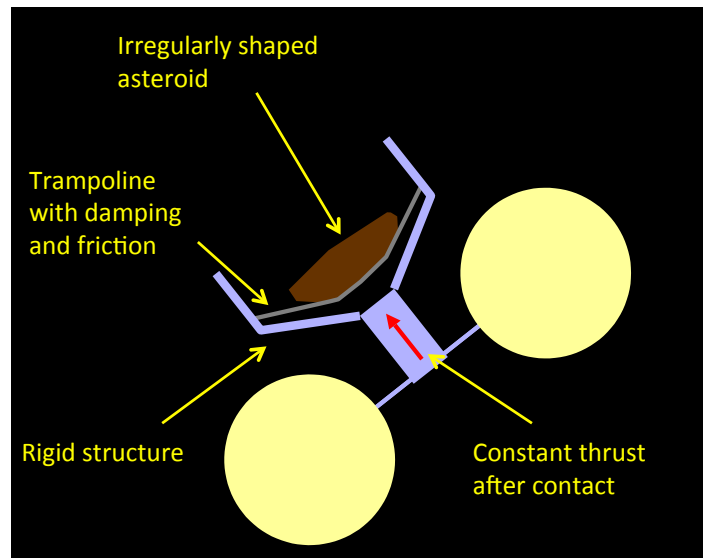


FIGURE 6. Illustration of spacecraft with trampoline capture device. Upon initial contact with the asteroid, the spacecraft applies constant thrust to maintain contact until the bag has been closed around the asteroid.

as the spacecraft adjusts itself to accommodate the asteroid shape after contact.

A natural strategy would be to perfectly match the motion of the asteroid and make contact at some pre-determined location with zero relative motion. However, this strategy is complicated in terms of GN&C and would consume a substantial amount of fuel. Two alternative approach strategies are discussed in [4]; one involves approaching along the angular momentum vector while spinning at a rate that approximately minimizes the relative motion, whereas the other involves matching the instantaneous angular velocity of the asteroid at the moment when contact is made (requiring precise timing and prediction of the asteroid motion).

One of the main goals of the trampoline capture design is to make the capture process more robust by minimizing sensitivity to the parameters of the approach. It is thought that the flexi-

bility of the trampoline fabric can absorb a significant amount of relative motion without imparting large forces on the spacecraft. Meanwhile, the constant thrust applied toward the asteroid is akin to an “artificial gravity,” and should allow the spacecraft to naturally accommodate the shape of the asteroid and settle against it in a stable configuration.

Asteroid Capture Simulation We use the trampoline model developed in the previous sections as part of an overall model for simulation of the dynamics of the asteroid capture process. In this model, the asteroid is represented as a rigid body with configurable inertial properties, and with a geometric shape described by an arbitrary triangle mesh. The spacecraft bus is modeled as a solid cylinder. The solar panels are modeled as solid cylinders on mass-less booms, connected to the bus via ball joints endowed with suitably parameterized spring-dampers. The trampoline is mounted from six suspension points, spaced 60° apart, attached to a rigid structure protruding from the spacecraft. Straightforward modifications to the trampoline model are made to account for the fact that the suspension points are no longer stationary, but instead move with the spacecraft. The spacecraft is subject to forces and torques equal and opposite to the ones imparted on the asteroid according to the trampoline model derived above.

The simulations are based on the *Darts/Dshell* architecture for spacecraft dynamics simulation, developed at JPL (see, e.g., [8]). The simulation runs at speeds faster than realtime on a desktop computer, and produces concurrent high-quality 3D visualizations of the capture.

SIMULATION RESULTS

Figure 7 shows a sequence of images from an example asteroid capture simulation in *Darts/Dshell*. The target is a 1000-t pear-shaped asteroid with a tri-inertial mass geometry, which is initialized with a spin rate of 0.5 RPM. The hexagonal trampoline has a nominal area of approximately 146 m^2 and is parameterized with $k = 1.5 \text{ N/m}^3$, $c = 15 \text{ Ns/m}^3$, and $\mu = 1.0$. The spacecraft approaches at 5 cm/s along the angular momentum vector, while flying in a corkscrew pattern to keep the asteroid geometrically centered within the bag. Upon contact, the spacecraft thrusts against the asteroid with a force of 475 N. The simulation is performed using a fourth-order Runge-Kutta integration method with a step size of 0.1 s. The SADA bending moments remain well within the acceptable limits in the course of the simulation.

Simulations were run with a number of different asteroids of different mass, shape, spin state, as well as different friction coefficients between the asteroid and the trampoline. The results show that the spacecraft tends to settle against the asteroid and catch up with its rotational motion. As expected, the constant

thrust results in the spacecraft orienting itself toward a stable configuration, typically resting on a flatter area of the asteroid.

For high-friction cases (μ close to 1.0), very little slippage between the asteroid and the trampoline is observed, and the spacecraft quickly catches up to the motion of the asteroid. For low-friction cases (μ close to 0.1), significant amount of slippage is observed, especially for asteroids with a relatively smooth surface, and the spacecraft takes longer to catch up to the motion of the asteroid.

As contact is maintained over several minutes, an interesting phenomenon is observed; namely, that the spacecraft tends to converge toward a “flat spin,” where the symmetry axis is roughly perpendicular to the axis of rotation of the overall system. This is unproblematic as long as the thrust level is chosen large enough to supply the necessary centripetal acceleration, and in fact it is desirable with respect to minimizing fuel consumption during the subsequent de-spin phase.

The loads on the spacecraft are generally small, and with an appropriately chosen thrust level after initial contact, the SADA bending moments remain well below critical levels.

CONCLUSIONS

In this paper we have presented a modeling technique that allows for fast simulation of asteroid capture using a capture device similar to a trampoline. As mentioned in the introduction, the technique involves a level of abstraction away from the actual mechanical implementation, in particular by assuming a certain potential energy and viscoelastic damping profile. Nevertheless, considerable freedom exists in bringing the model and the physical mechanism into alignment, both by modifying the energy profiles assumed in this paper and by modifying the physical motor profiles at the trampoline suspension points.

Visually, the model produces realistic results; however, validation against physical or higher-fidelity models would be necessary to confirm that the model captures the dynamics of the spacecraft-asteroid system with sufficient accuracy. Moreover, extensive Monte-Carlo simulations would be needed to build confidence in the overall technical solution. We refer readers to a separate paper [9] for a description of one-fifth scale hardware-in-the-loop asteroid capture test bed built at JPL as part of the Option A study.

ACKNOWLEDGMENT

The research described in this paper was carried out at the Jet Propulsion Laboratory, California Institute of Technology, under a contract with the National Aeronautics and Space Administration. We would like to thank the members of the capture mechanism design and GN&C teams, with special thanks to Brian Wilcox (capture mechanism design lead).

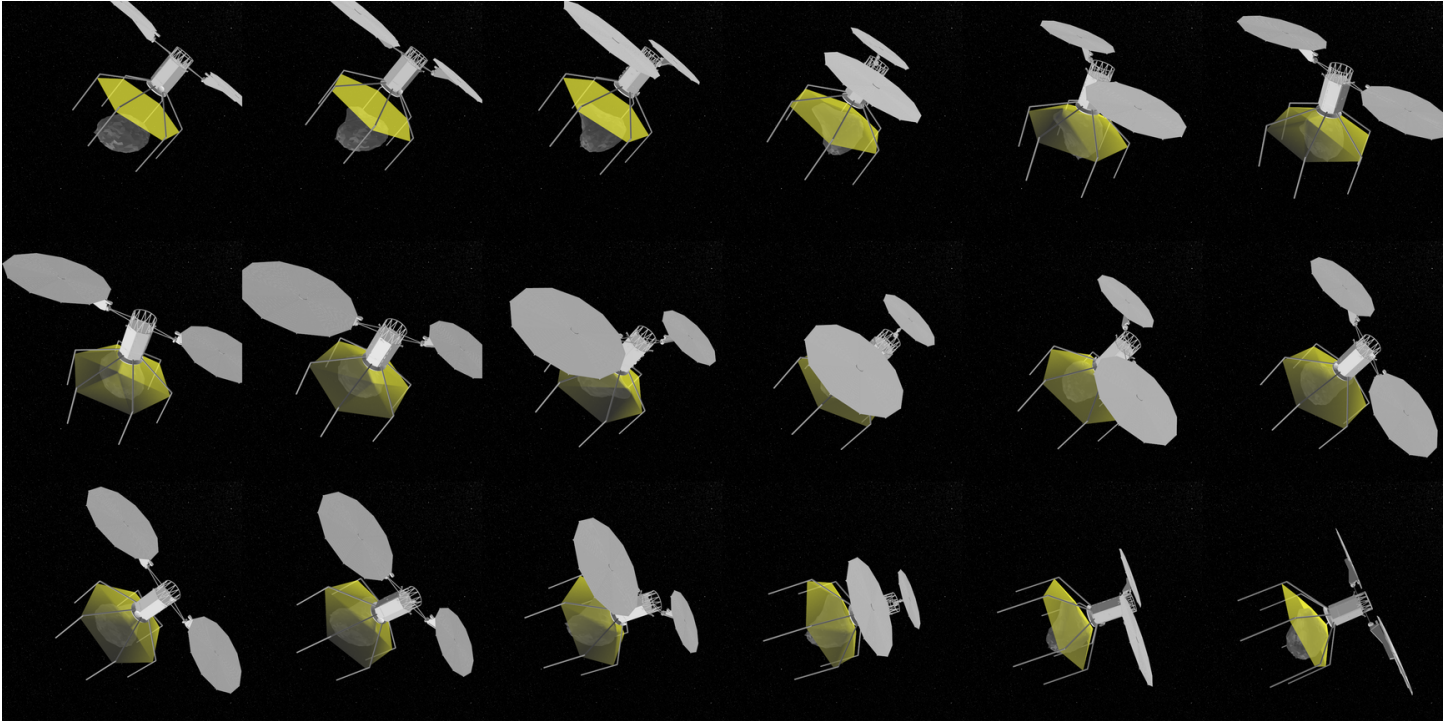


FIGURE 7. Excerpt from an example Darts/Dshell simulation of an asteroid capture. The spacecraft approaches a pear-shaped asteroid at 5 cm/s while flying a corkscrew pattern to keep the asteroid geometrically centered in the bag. The images show the period from $t = 0$ s to $t = 170$ s in 10 s increments, in order from top left to top right, continuing from middle left to middle right and from bottom left to bottom right.

REFERENCES

- [1] Burns, J. A., and Safronov, V. S., 1973. “Asteroid nutation angles”. *Monthly Notices of the Royal Astronomical Society*, **165**, pp. 403–411.
- [2] J. Brophy, F. Culick, F. Friedman, et al., 2012. Asteroid retrieval feasibility study. Tech. rep., Keck Institute for Space Studies, California Institute of Technology, 04.
- [3] Van Gelder, A., 1998. “Approximate simulation of elastic membranes by triangulated spring meshes”. *J. Graphics Tools*, **3**(2), pp. 21–42.
- [4] Grip, H. F., Ono, M., Balaram, J., Cameron, J., Jain, A., Kuo, C., Myint, S., and Quadrelli, M., 2014. “Modeling and simulation of asteroid retrieval using a flexible capture mechanism”. In Proc. IEEE Aerospace Conf.
- [5] Anitescu, M., and Potra, F. A., 1997. “Formulating dynamic multi-rigid-body contact problems with friction as solvable linear complementarity problems”. *Nonlinear Dynamics*, **14**(3), pp. 231–247.
- [6] Trinkle, J. C., 2003. “Formulation of Multibody Dynamics as Complementarity Problems”. In ASME International Design Engineering Technical Conference.
- [7] Mylapilli, H., and Jain, A., 2014. “Evaluation of Complementarity Techniques for Minimal Coordinate Contact Dynamics”. In Proceedings of the ASME 2014 International Design Engineering Technical Conferences & Computers and Information in Engineering Conference.
- [8] Lim, C., and Jain, A., 2009. “Dshell++: A component based, reusable space system simulation framework”. In Proc. Third IEEE International Conference on Space Mission Challenges for Information Technology.
- [9] Wilcox, B., Litwin, T., Carlson, J., Shekels, M., Grip, H. F., Jain, A., Lim, C., Myint, S., Dunkle, J., Sirota, A., Fuller, C., and Howe, A. S., 2015. “Testbed for studying the capture of a small, free-flying asteroid in space”. In Proc. AIAA SPACE Forum 2015. Submitted.